Available online at www.sciencedirect.com
ScienceDirect
Micron 38 (2007) 354–361
micron
www.elsevier.com/locate/micron

Valence state map of iron oxide thin film obtained from electron spectroscopy imaging series

Ko-Feng Chen [a], Shen-Chuan Lo [b], Li Chang [c], Ray Egerton [d], Ji-Jung Kai [a], Juhn-Jong Lin [e], Fu-Rong Chen [a,f,*]

[a] *Department of Engineering and System Science, National Tsing Hua University, HsinChu 30013, Taiwan*
[b] *Microstructure and Characterization Laboratory, Materials Research Laboratories, Industrial Technology Research Institute, HsinChu 31040, Taiwan*
[c] *Department of Materials Science and Engineering, National Chiao-Tung University, HsinChu 30010, Taiwan*
[d] *Department of Physics, University of Alberta, Edmonton, Canada T6G 2J1*
[e] *Department of Electrophysics, National Chiao Tung University, HsinChu 30010, Taiwan*
[f] *National Synchrotron Radiation Research Center, HsinChu 30076, Taiwan*

Abstract

This paper demonstrates the applicability of electron-spectroscopic imaging (ESI) for valence-state mapping of the iron oxide system. We have previously developed a set of signal-processing methods for an ESI series, to allow mapping of sp^2/sp^3 ratio, dielectric function and energy bandgap. In this study, these methods are applied to generate a valence-state map of an iron oxide thin film (Fe/α-Fe_2O_3). Two problems, data undersampling and a convolution effect associated with extraction of the image-spectrum from the core loss image series, were overcome by using cubic-polynomial interpolation and maximum-entropy deconvolution. As a result, the reconstructed image-spectrum obtained from the ESI series images has a quality as good as that of conventional electron energy-loss spectra. The L_3/L_2 ratio of the reconstructed ESI spectrum is determined to be 3.30 ± 0.30 and 5.0 ± 0.30 for Fe and α-Fe_2O_3, respectively. Our L_3/L_2 ratio mapping shows an accurate correspondence across the Cu/Fe/α-Fe_2O_3 region. The effect of delocalization and chromatic aberration on the ESI resolution is discussed and estimated to be about 2 nm for the case of L_3/L_2 ratio mapping.

Keywords: Valence state map; Electron spectroscopic imaging(ESI); Iron oxide system; Electron energy-loss spectroscopy(EELS)

1. Introduction

The Fe–O system is widely used in many applications, such as magnetic recording devices (Snoeck et al., 2004) and in contrast agents for magnetic-resonance imaging (Wang et al., 2001), but there are several varieties of iron oxide compounds with different structures and properties. For example, Fe_3O_4 (ferrite) has an inverse spinel structure, and is ferromagnetic, whereas α-Fe_2O_3 has a hexagonal structure, and is antiferromagnetic. These oxides, in the form of thin films and nanostructures, are increasingly developed for technological applications. Therefore, how to quantify the iron oxide compound is an important consideration for processing and device development.

"White Lines" are characteristic features often observed in the electron energy-loss spectrum (EELS) of transition metals and rare-earth metals. They are intense sharp peaks at the onset of the ionization edge, arising because there are unoccupied states in the M- or N-shell (d- or f-bands in a solid). The white-line intensity ratio can be applied to investigate the valence state of these metals, as has been demonstrated in several papers (Colliex et al., 1991; Van Aken and Liebscher, 2002; Wang et al., 1997). As a result, energy-loss near-edge structures (ELNES) can be used as valence fingerprints to provide chemical information. Table 1 gives the white-line intensity ratios for different transition metals and shows that the variation in L_3/L_2 ratio between the different oxides is smallest for the Fe–O system. Beware that there is a small deviation in the L_3/L_2 ratio for the α-Fe_2O_3 system as determined by different groups (Colliex et al., 1991; Van Aken and Liebscher, 2002). This small difference may originate from the model chosen to isolate the white lines from the underlying transitions to unoccupied continuum states, as discussed by Van Aken and Liebscher (2002).

* Corresponding author.
E-mail address: frchen@ess.nthu.edu.tw (F.-R. Chen).

0968-4328/$ – see front matter © 2006 Published by Elsevier Ltd.
doi:10.1016/j.micron.2006.06.004

Table 1
Table of the white line L_3/L_2 intensity ratios for different transition metals

	Fe–O system				
	Fe	FeO	Fe_3O_4	γ-Fe_2O_3	α-Fe_2O_3
L_3/L_2 ratio [6]	3.8 ± 0.3	4.6 ± 0.3	5.2 ± 0.3	5.8 ± 0.3	6.5 ± 0.3
L_3/L_2 ratio [7]		3.6–3.7			5.2–5.3
	Co–O system				
	Co^{2+}		$(1/3)Co^{2+} + (2/3)Co^{3+}$		Co^{4+}
L_3/L_2 ratio [8]	5 ± 0.25		3.45 ± 0.2		2 ± 0.2
	Mo–O system				
	Mn^{2+}		Mn^{3+}		Mn^{4+}
L_3/L_2 ratio [8]	4.3 ± 0.2		2.3 ± 0.15		1.95 ± 0.15

Although energy-filtered transmission electron microscopy (EFTEM) provides a rapid and efficient method for qualitative characterization from two-dimensional maps by use of the two- or three-window techniques (Egerton, 1996; Reimer, 1995), the chemical bonding and electronic structure can only be analyzed quantitatively by electron energy-loss spectrometry. Two spectroscopic imaging methods have been developed to implement this. The first technique, known as the spectrum-imaging method, is to acquire a two-dimensional EELS spectrum by scanning the focused electron beam across the sample, as proposed by Jeanguillaume and Colliex (1989). The other method is electron-spectroscopic imaging (ESI) or image spectroscopy, which extracts the spectrum at a specific position from a series of energy-loss images (Jeanguillaume et al., 1978). The advantage of the spectrum-imaging method is that the energy resolution, 0.3–1 eV depending on the type of electron gun and the accelerating voltage, is better than for electron spectroscopic imaging (ESI), which gives 4–20 eV depending on the width of the energy-selecting slit. The major disadvantage of spectrum imaging is a longer acquisition time than required by the ESI method (Yang et al., 2002).

In the ESI method, the derived spectrum is convolved in energy with the energy-selecting slit, which causes the energy resolution to be worse. In order to solve this convolution effect, a maximum-entropy deconvolution method (Yang et al., 2002; Lo et al., 2001; Tsai et al., 2004) is introduced. However, a problem of undersampling, due to the limited energy dispersion, must be taken into account. The undersampling problem arises because the energy-selecting slit is moved in discrete energy increments to reduce the acquisition time, therefore the technique of interpolation is also introduced. A set of signal processing methods for an electron spectroscopic image (ESI) series has been previously developed for the mapping of the dielectric function (Lo et al., 2001), sp^2/sp^3 ratio (Yang et al., 2002) and energy bandgap (Tsai et al., 2004). In this paper, we extend our previous methods (for the valence-state mapping in the core-loss region) to energy losses that are substantially higher than in these previous publications.

Valence-state distributions of Mn and Co, using white-line intensity ratios in energy-filtered TEM, have been demonstrated by Wang et al. (2000). A five-window technique was used: first two images acquired prior the L_3 peak are used to subtract the background, two images are acquired from the L_3 and L_2 white lines, and fifth image is acquired to subtract the continuous background underneath the L_3 and L_2 peaks. The difference between Wang's method and ours is that many more images are acquired in the ESI method. Statistically, more data points in the reconstructed EEL spectra allow better estimates of the pre-edge background (by the power-law AE^{-r} method) and of the white-line background (due to transitions from initial to continuum states, subtracted using a double arctangent). These better estimates should yield a more precise analysis of the white-line intensity ratio. Therefore, it is envisaged that more precise spectra can be reconstructed from an ESI series images, leading to a better quantification of the valence state. On the other hand, a longer time is needed to acquire the ESI series and specimen drift will be more serious. Even so, it will be shown that the ESI-extracted white-line spectra can have the same quality as those acquired by electron-probe EELS.

2. Experiment

A sample with the structure: α-Fe_2O_3/Fe/Cu/Si-substrate, shown in Fig. 1(a), was employed for the valence state

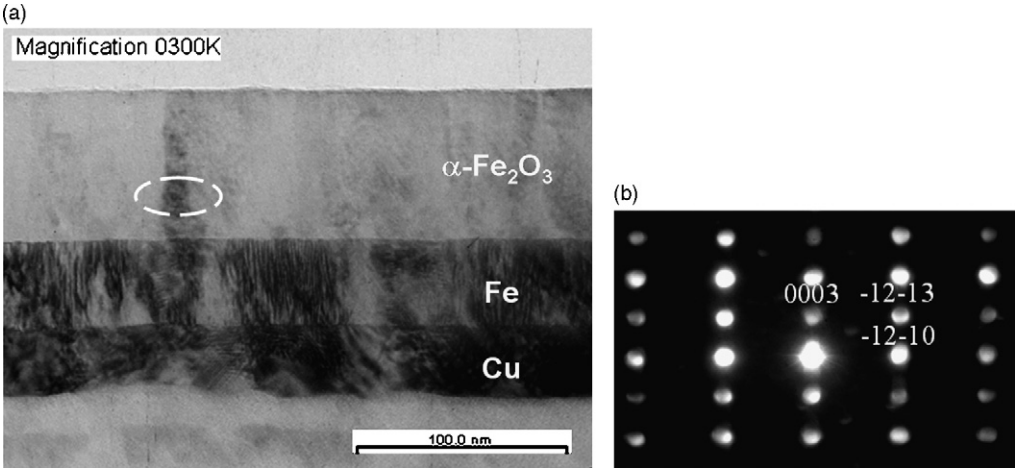

Fig. 1. (a) TEM micrograph showing the structure of the Cu/Fe/α-Fe_2O_3 specimen. (b) Diffraction pattern of the circular area in (a) the zone axis is along [1 0 $\bar{1}$ 0].

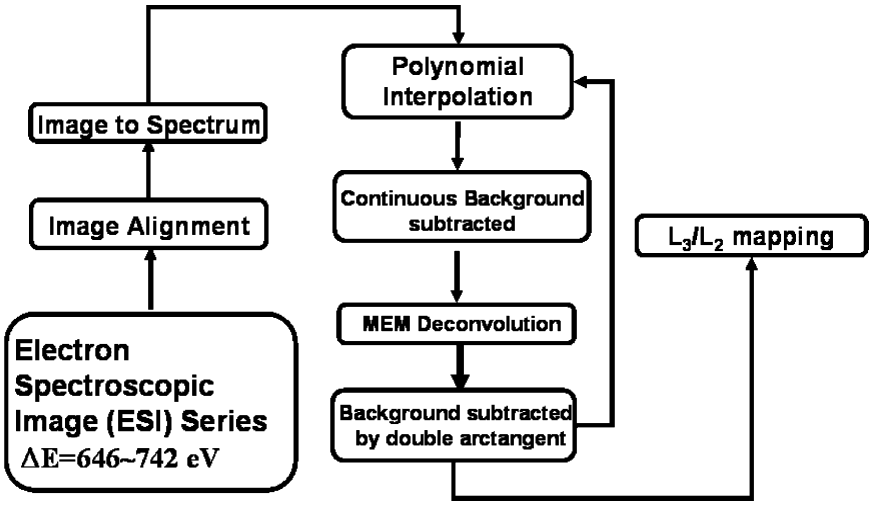

Fig. 2. Flow chart of the signal processing procedures for reconstructing ESI spectra and valence state mapping.

mapping. It was prepared by reactive-ion sputtering. In the Fe–O system, the L_3/L_2 ratios are 3.8, 4.6, 5.2, 5.8 and 6.5 for Fe, FeO, Fe_3O_4, γ-Fe_2O_3 and α-Fe_2O_3, respectively (Colliex et al., 1991). The variation of L_3/L_2 ratio between different iron oxide compounds is in the range of 0.6–0.8, which is smaller than other transition metal oxides. Therefore, in the Fe–O system, the accuracy of the white line intensity ratio is quite important and statistical fluctuations recorded from the same compound should be made as small as possible. From the diffraction pattern shown in Fig. 1(b), it can be identified that the upper layer is α-Fe_2O_3. The thicknesses of the multilayered Fe/α-Fe_2O_3 samples are 40 and 70 nm, respectively, and the thickness of the specimen was 100 nm, measured by low-loss EELS (Egerton, 1996).

In this study, we used a JEOL 2100F transmission electron microscope, operated at 200 kV and equipped with Schottky-type gun and a Gatan imaging filter. Electron spectroscopic image series were recorded on a Gatan 1024 × 1024 slow-scan charge-coupled-device (CCD) camera. The ESI series was recorded from 646 to 742 eV loss in steps of 4 eV. The width of the energy-selecting slit was also 4 eV, which is larger than that used in our previous papers, namely 1 eV for low-loss spectra and 2 eV for the carbon K-edge. In the core-loss region, the inelastic scattering cross-section is lower than that in the low-loss region; therefore a larger width of the energy-selecting slit and energy step were chosen to ensure a sensible balance between signal/noise, contamination and radiation damage. The exposure time of each image was 35 s and the collection semi-angle β was 15.8 mrad. The pixel resolution in the ESI series was 0.4 nm per pixel, calibrated from the magnification. The spectra were extracted from a square area of 5 × 5 pixels, corresponding to 2 nm × 2 nm.

The extracted spectra were processed by a set of signal-processing programs consisting of polynomial interpolation, background subtraction and maximum-entropy deconvolution. In order to obtain a better sampling for the deconvolution process, polynomial interpolation was employed. The maximum entropy deconvolution method (MEM) has been adopted to overcome the convolution effect resulting from the ESI series acquired with a finite energy window. The details of the process for the reconstruction of ESI spectra can be found in our previous publications. A flow chart of the analytical procedure is given in Fig. 2. All of the programs were written using Digital Micrograph script and Matlab language.

3. Algorithm for white-line intensity ratio

"White lines" are the famous features observed in the EELS of transition metals and rare-earth metals. For a transition metal, they are composed of L_3 and L_2 peaks, which represent transitions from $2p^{3/2}$ and $2p^{1/2}$ initial states to $3d^{3/2}$ and $3d^{5/2}$ final states (Van Aken and Liebscher, 2002). In order to acquire the white-line intensity ratio, the effect of transitions from $2p^{3/2}$ and $2p^{1/2}$ initial states to the continuum states, $nd^{3/2}$ and $nd^{5/2}$, which still obey the selection rule: $\Delta\ell = \pm 1$, must be subtracted.

The double arctangent function shown below is used as the background function:

$$f(E) = \frac{h_1}{\pi} \times \left[\arctan(\pi \cdot (E - E_1)) + \frac{\pi}{2}\right] + \frac{h_2}{\pi} \times \left[\arctan(\pi \cdot (E - E_2)) + \frac{\pi}{2}\right] \quad (1)$$

Here h_1, h_2 are the heights of the two arctangent functions, which are the minima behind the L_3 and L_2 edges. The E_1 and E_2 are the positions of L_3 and L_2 edges, and E is the energy loss. After subtraction of double arctangents, two Lorentzian functions associated with the L_2 and L_3 will result. The ratio of L_3/L_2 can be calculated from the ratio of integrated intensity $I(L_3)/I(L_2)$ under the Lorentzian functions, as expressed in the following equation:

$$\frac{I(L_3)}{I(L_2)} = \frac{\int_{L_3-w/2}^{L_3+w/2} I(E)\,\mathrm{d}E}{\int_{L_2-w/2}^{L_2+w/2} I(E)\,\mathrm{d}E} \quad (2)$$

where L_3 and L_2 are the centers of the Lorentzian functions and w is the integration window. The width of the L_3 or L_2 peak for

both Fe and α-Fe_2O_3 is about 4 eV in the reconstructed ESI spectrum, therefore an integration window of 4 eV is chosen to integrate the total Fe $L_{2,3}$ white-line intensity ratio.

4. Results and discussion

4.1. Processing of extracted ESI spectrum

Fig. 3(a) is an unfiltered image of the specimen. In order to avoid strong diffraction conditions, the dashed line area (24 nm × 100 nm) in the field of view was tilted away from any zone axes and selected for valence-state mapping. Fig. 3(b) is an ESI series that has been aligned and obtained from the dashed line area in Fig. 3(a). Fig. 3(c) and (d) are typical extracted spectra of Fe and α-Fe_2O_3 layers. The energy dispersion of the two spectra is 4 eV per channel. Two peaks, L_3 and L_2, can be seen in each spectrum. We can distinguish Fe and α-Fe_2O_3 spectra easily because they have two different characteristics. First, the maximum intensity associated with L_3 edge in the Fe spectrum is at 706 eV whereas that in α-Fe_2O_3 is at 710 eV. The other characteristic is that the tail of the Fe spectrum is higher than that of the α-Fe_2O_3 spectrum.

In order to reconstruct the ESI spectrum, it is necessary to interpolate the as-extracted spectra, giving lower eV/channel, in order to obtain a better result in the deconvolution procedure. In our previous publication (Yang et al., 2002; Lo et al., 2001; Tsai et al., 2004), FFT (Fast Fourier Transformation) interpolation was used to improve the energy dispersion because of its characteristic of model independence. The FFT interpolation usually works better for a smooth spectrum, although in the case of sharply rising peaks, enough sampling data points are required. In this study, a cubic polynomial interpolation was employed because artifacts in the area between the sharp rising edges of L_2 and L_3 (caused by the FFT interpolation) could not be eliminated due to insufficient sampling in this energy region. Fig. 4 is the Fe spectrum; the circled line is the spectrum extracted from ESI images and the dotted line is the cubic polynomial-interpolated spectrum. The dispersion of the as-extracted ESI spectra was 4 eV per channel and that of interpolated spectra was 0.2 eV per channel. As we see, the cubic polynomial-interpolated spectrum follows the same trend as the as-extracted spectrum.

The spectra were then processed by a set of signal-processing programs, consisting of background subtraction and

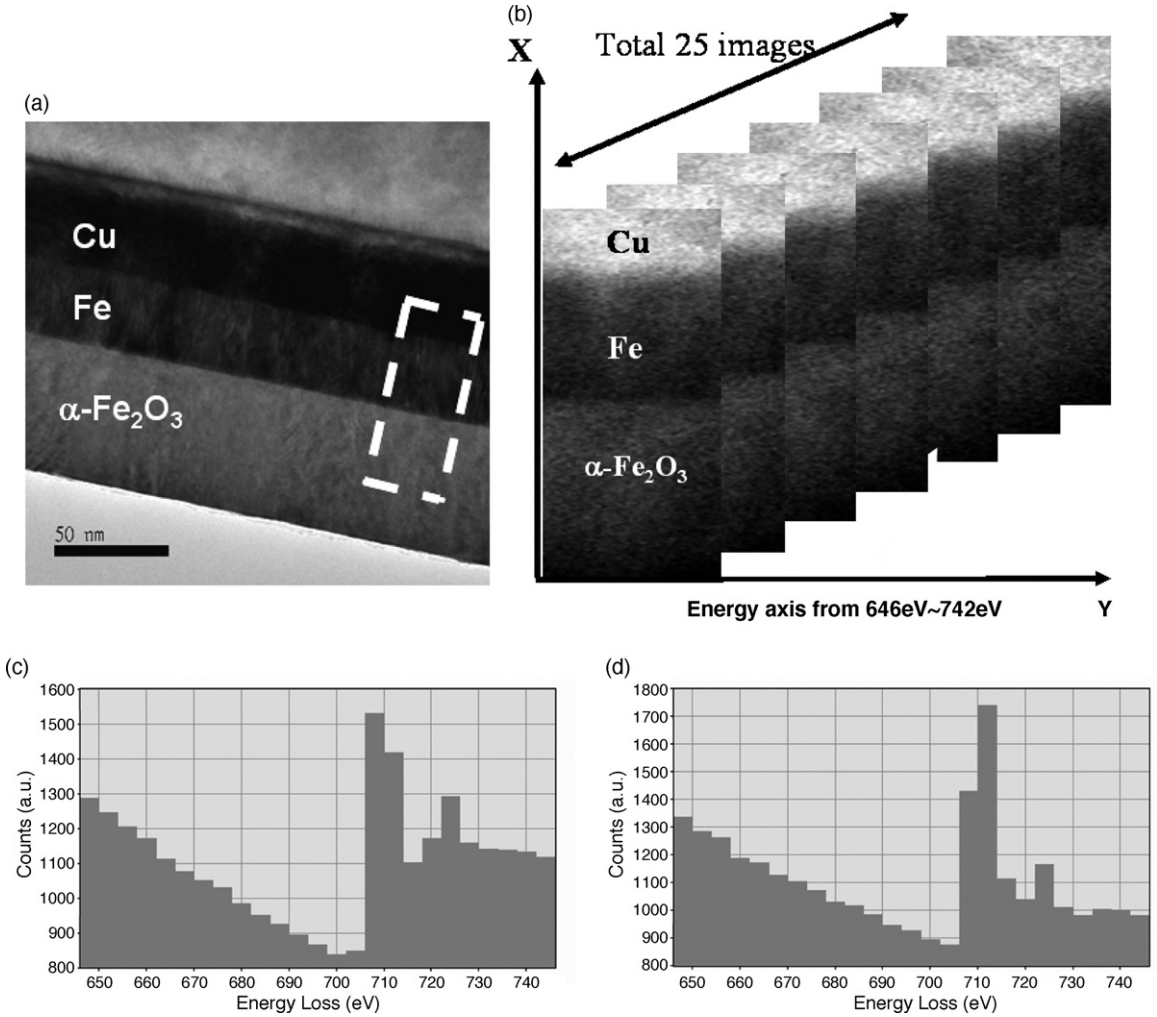

Fig. 3. (a) Unfiltered image of the specimen. (b) ESI series acquired from energy loss between 646 and 742 eV, corresponding to the dashed line area of (a). As-extracted spectra of Fe and α-Fe_2O_3 are shown in (c) and (d), respectively.

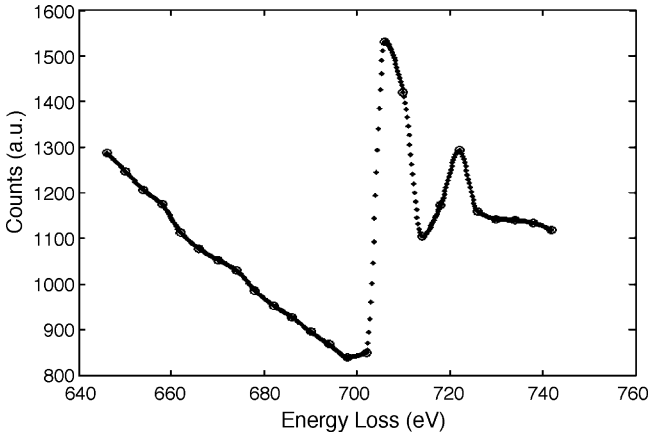

Fig. 4. The circled line is the as-extracted spectrum of Fe from ESI images and the dotted line is the spectrum interpolated by polynomial interpolation.

maximum-entropy deconvolution. Fig. 5 shows typical reconstructed spectra of Fe and α-Fe_2O_3. The average positions of the L_3 edge from the area of Fe and α-Fe_2O_3 films are 707.6 ± 0.5 and 709.0 ± 0.5 eV, while those of L_2 peaks are 721.6 ± 0.5 and 722.4 ± 0.5 eV. Previous references (Leapman et al., 1982; Van Aken and Liebscher, 2002) give the L_3 edge of Fe and α-Fe_2O_3 at 706 and 709.5 eV, and the L_2 edge at 719.2 and 722.6 eV. As can be seen, the positions of L_3 and L_2 edges of reconstructed spectra associated with α-Fe_2O_3 are close to those previously reported (within experimental error ±0.5 eV), while those associated with Fe deviate by a slightly larger error from the references. The energy separations of L_3 and L_2 edges for Fe and α-Fe_2O_3 are 13.2 and 13.1 eV from reported references (Colliex et al., 1991), while the average energy separations in reconstructed ESI spectra are at 14 and 13.4 eV, respectively, which are in good agreement with the previously reported data within experimental error. The energy separation of the L_3 and L_2 edges for Fe and α-Fe_2O_3 is about three times larger than the 4 eV width of energy slit, indicating that the slit used in acquiring the ESI spectra enables the L_3 and L_2 edges in

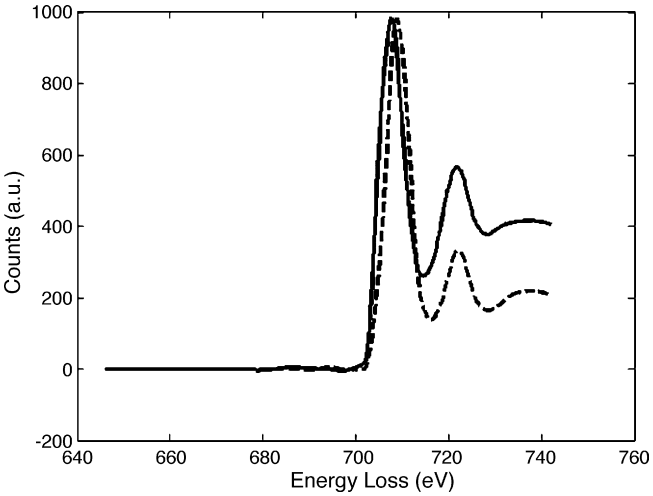

Fig. 5. Reconstructed spectra from α-Fe_2O_3 (dashed line) and Fe (real line). The energy difference between the L_3 peaks of Fe and α-Fe_2O_3 is 1.4 eV.

reconstructed ESI spectra to be resolved sufficiently for quantitative analysis of L_3/L_2 ratio.

Fig. 6(a) and (b) are the reconstructed ESI and probe-acquired spectra of Fe and α-Fe_2O_3, respectively. In order to compare the reconstructed ESI spectra and the probe spectra conveniently, these spectra have been aligned at the energy loss corresponding to the L_3 peak, 707 eV for Fe spectra and 710 eV for α-Fe_2O_3 spectra. The dashed lines are the probe spectra, acquired with the electron probe size set to 0.5 nm, and the real lines are the reconstructed ESI spectra. For Fe, the energy differences between the L_3 and L_2 edges are 13.6 and 14 eV for probed spectra and reconstructed ESI spectra, respectively. For α-Fe_2O_3 spectra, this energy difference is 13.4 eV for both of probed spectra and reconstructed ESI spectra. Although the energy step is 4 eV in this experiment, the reconstructed ESI spectra are consistent with the probe spectra. Not only that, but the relative intensity of the spectra, after normalizing the probe and reconstructed ESI spectra, are highly consistent, which is very important for the valence-state quantification. In short, the set of signal-processing methods for an electron spectroscopic image (ESI) series successfully reconstructs the energy-loss spectrum.

The chemical shift of the L_3 edge is one of the methods available to quantify the valence states of the transition metal oxides. For example, there is a chemical shift of 1.7 eV between Fe^{3+} and Fe^{2+}, whose maximum intensity of L_3 edge is located in 709.5 and 707.8 eV, respectively (Van Aken and Liebscher, 2002). However, the energy resolution of spectra should be as good as 0.1–0.2 eV if we want to quantify the valence states in the case of mixed valence states. In the ESI system, the energy-selecting slit is usually wider than 1 eV to avoid radiation damage when measuring the core loss region; therefore the energy resolution will be worse than 1 eV. As a result, quantification of the valence states by chemical shift of the L_3 peak is not an appropriate method. However, quantification using the white-line intensity ratio is suitable because it does not require such a good energy resolution. The L_3/L_2 ratio has little dependence on the specimen thickness, as reported by Wang et al. (2000). This is because the energies of the characteristic plasmon peaks are larger than the energy difference between the L_3 and L_2 peaks, so that multiple scattering (plasmon + core loss) has little effect on the near-edge structure. Therefore we did not execute Fourier-ratio deconvolution to retrieve single-scattering spectra in this experiment.

4.2. Quantification of L_3/L_2 ratio from processed image spectra

Fig. 7(a) is the area selected for the analysis of valence state mapping and corresponds to a dashed line area in Fig. 3(a). The total area is 24 nm × 100 nm, and the spectra were extracted from a square area of 2 nm × 2 nm, so there are 12 × 50 points to be analyzed for the valence-state map. Every image point was processed through the set of signal-processing methods, as mentioned in the earlier section. After subtraction of the double-arctangent function, given in Eq. (1), from the

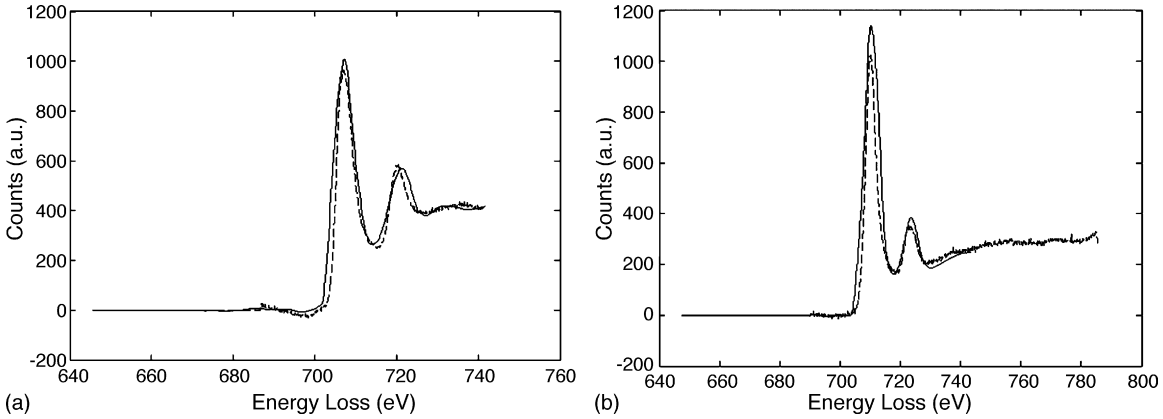

Fig. 6. (a) and (b) are spectra of Fe and α-Fe_2O_3, respectively. The dashed line is the probe spectrum and the real line is the ESI signal-processed spectrum.

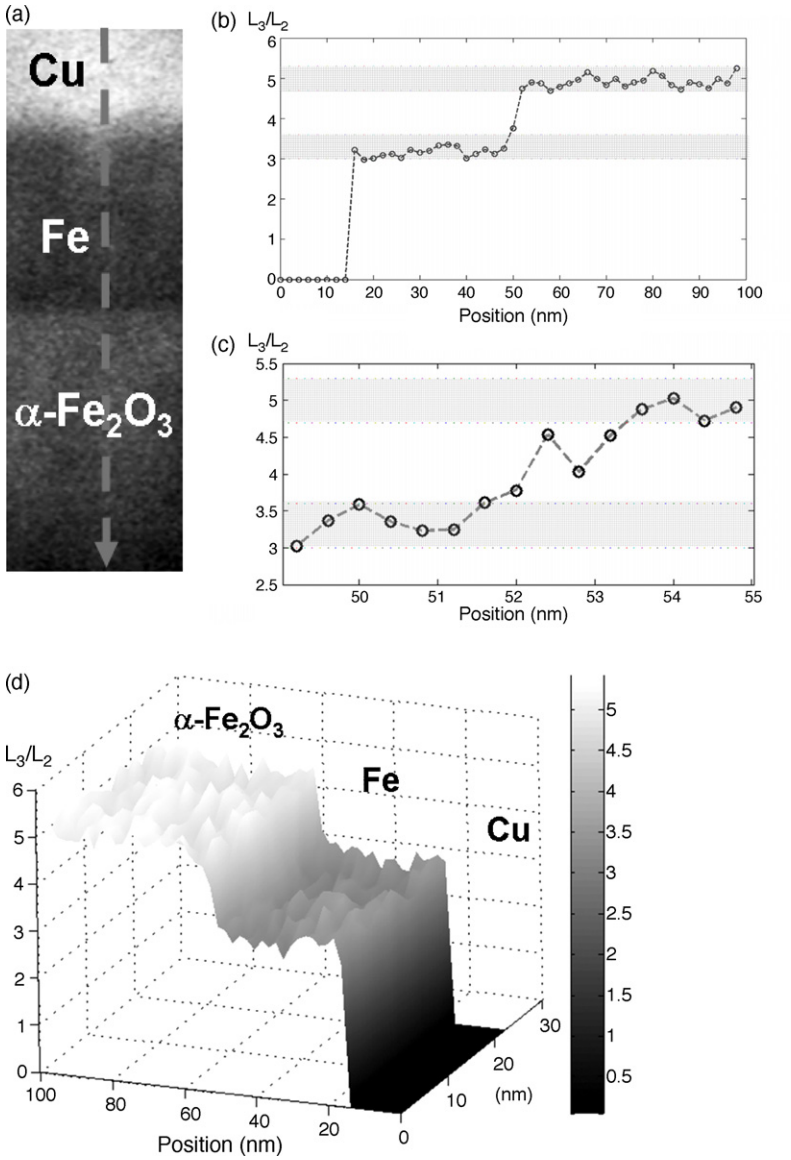

Fig. 7. (a) Area selected for the valence state mapping. (b) Line scan of valence state, along the position corresponding to the dashed line in (a). The spectra are extracted from 2 nm × 2 nm. (c) Line scan of valence state, corresponding to the interface between Fe and α-Fe_2O_3 in (b). The spectra are extracted from 0.4 nm × 2 nm, which are parallel to the interfaces. The shadow areas in (b) and (c) are corresponding to the distribution range of L_3/L_2 ratio in different states of oxides. In (d) we show the valence state map corresponding to (a).

Table 2
List of the results for reconstructed ESI spectra and probed spectra

	Energy difference, $E_{L_2} - E_{L_3}$ (eV)	L_3/L_2 ratio	Chemical shift between Fe and α-Fe_2O_3 (eV)
Probe spectrum			
Fe	13.6	3.32	3
α-Fe_2O_3	13.4	5.21	
Reconstructed ESI spectrum			
Fe	14	3.30 ± 0.3	1.4
α-Fe_2O_3	13.4	5.0 ± 0.3	

reconstructed ESI spectrum, typical Lorentzian functions were fitted to the L_3 and L_2 edges for both Fe and Fe_2O_3. The L_3/L_2 ratio can then be calculated using Eq. (2).

Fig. 7(d) is a valence state map corresponding to Fig. 7(a): the z-axis is the L_3/L_2 ratio, and the x–y plane corresponds to the area of Fig. 7(a). The L_3/L_2 ratios of Cu, Fe and α-Fe_2O_3 are 0, 3.3 ± 0.3 and 5.0 ± 0.3, respectively. There is no peak for Cu in the L_3/L_2 region of iron, so after background subtraction the intensity of the Cu spectra is almost equal to zero. In order to distinguish three layers clearly in the valence-state map, the L_3/L_2 ratio of Cu is set as zero. The variation range (± 0.3) is the statistical variation from the whole valence-state map. As mentioned in the earlier section, there is a small deviation in the L_3/L_2 ratio for the α-Fe_2O_3 system determined by different groups: 6.5 ± 0.3 (Colliex et al., 1991) and 5.2–5.3 (Van Aken and Liebscher, 2002). The small difference may arise from the different models for transitions to unoccupied continuum states, as discussed by Van Aken and Liebscher (2002). The average L_3/L_2 ratio for α-Fe_2O_3 deduced from our ESI spectra is close to that given by Van Aken and Liebscher (2002). Despite this deviation in the reported L_3/L_2 ratio for the α-Fe_2O_3 system, the accuracy of ESI spectral analysis is sufficient to clearly distinguish the valence states of α-Fe_2O_3 and of Fe, allowing us to easily distinguish three different layers in Fig. 7(d).

Table 2 gives our results for reconstructed ESI spectra and probe spectra. The L_3/L_2 ratios of Fe are 3.32 and 3.30 ± 0.3 for probed and ESI spectra, respectively, whereas the L_3/L_2 ratios of α-Fe_2O_3 are 5.21 and 5.0 ± 0.3 for the probe and ESI spectra. Although, there is slight difference in L_3/L_2 ratio deduced from probe and reconstructed ESI spectra, this difference is within the statistical error of ± 0.3, which is smaller than achieved by other valence state map methods (Wang et al., 2000). The white-line ratios acquired from the signal-processing ESI method in our experiment can be as standards to quantify other cases, for example of mixed valence states. Fig. 7(b) is a line scan of L_3/L_2 ratio, which corresponds to the dashed line in Fig. 7(a). The shadow areas are corresponding to the distribution range of L_3/L_2 ratio for Fe and α-Fe_2O_3. The half-width of the profile at the interface is 1 pixel, which corresponds to a resolution of about 2 nm.

4.3. Spatial-resolution limits

A delocalization effect, which limits the resolution of EFTEM images, has been discussed previously (Muller and Silcox, 1995; Krivanek et al., 1995; Egerton, 2003). Delocalization of inelastic scattering occurs because probe electrons that pass within a certain distance (called as impact parameter b) of the target electron can still ionize the atom. The delocalization distance can be expressed (Egerton, 2003) as:

$$d_{\mathrm{d}} = 0.5\lambda/\theta_{\mathrm{E}}^{3/4} \tag{3}$$

where λ is the wavelength of the electron, $\theta_{\mathrm{E}} = \Delta E/2E_0$ the characteristic angle of inelastic scattering and ΔE the energy loss. As seen from Eq. (3), delocalization is more significant at low values of energy loss and there are three other factors that should be considered in the core-loss region, namely the diffraction limit, chromatic aberration of the objective lens and spherical aberration of the objective (Egerton and Crozier, 1997).

The resolution limit due to chromatic aberration is given by $2(r_{50})_{\mathrm{c}}$, where $(r_{50})_{\mathrm{c}}$ is the radius containing 50% of the electrons, which is about 30% of the total radius r_{c} of the total spreading due to chromatic aberration:

$$(r_{50})_{\mathrm{c}} \approx 0.3 r_{\mathrm{c}} \tag{4}$$

Here $r_{\mathrm{c}} = (C_{\mathrm{c}}/E_0)(w/2)\beta$, where β is the collection angle, C_{c} the chromatic aberration coefficient and E_0 the electron energy and w is energy-slit width.

The resolution limit due to spherical aberration is given by $2(r_{50})_{\mathrm{s}}$, where $(r_{50})_{\mathrm{s}}$ is the radius containing 50% of the electrons and is about 6.5% of the PSF radius r_{s} for a thin specimen and Fe L-loss electrons:

$$r_{50} \approx 0.065 r_{\mathrm{c}} \tag{5}$$

The value $r_{\mathrm{c}} = C_{\mathrm{s}}\beta^3$ represents the overall radius of the PSF, where C_{s} is the spherical aberration coefficient of the objective lens.

The resolution limit due to diffraction (caused by the objective aperture) is given by:

$$d_{\mathrm{diff.}} = 0.6\lambda/\beta \tag{6}$$

The total resolution limit is then expressed as:

$$d_{\mathrm{total}} = \left(d_{\mathrm{d}}^2 + d_{\mathrm{diff.}}^2 + (2r_{50})_{\mathrm{c}}^2 + (2r_{50})_{\mathrm{s}}^2\right)^{1/2} \tag{7}$$

We evaluated Eqs. (3)–(6) with following parameters: $\Delta E = 700$ eV, $E_0 = 200$ keV, $C_{\mathrm{c}} = 1.1$ mm, $C_{\mathrm{s}} = 0.5$ mm, $\beta = 15.8$ mrad and w (slit width) = 4 eV, giving resolution limits due to delocalization, chromatic aberration, spherical aberration and diffraction (due to the objective aperture) as 0.15, 0.35, 0.26 and 0.1 nm, respectively. Combining these terms according to Eq. (7), the theoretical EFTEM spatial resolution is 0.47 nm. Therefore it appears that our measured spatial resolution (2 nm) is determined by the pixel size used in the experiment.

In order to estimate the spatial resolution more accurately, spectra extracted from a smaller area (0.4 nm × 2 nm) parallel to the interface were acquired. The extracted spectra were processed the same signal-processing methods as mention above. The line scan between Fe and α-Fe_2O_3 interface is shown in Fig. 7(c). The half-width of the profile at the interface

is 3 pixels, which corresponds to a resolution of ∼1.2 nm, which is still larger than theoretical value, probably due to specimen drift.

5. Conclusion

A set of signal processing methods, consisting of polynomial interpolation, background subtraction and maximum-entropy deconvolution, has been successfully developed for valence-state mapping of the iron oxide system. The ESI-reconstructed energy-loss spectrum is in good agreement with the probe-acquired spectrum. The L_3/L_2 ratio of the ESI-reconstructed spectrum is accurate within the range of ±0.3, which is adequate for quantification of the valence state. The white line ratios of Fe and α-Fe_2O_3 are 3.3 and 5.0, which can be taken as standard values for quantification by the signal-processing ESI method (using 4 eV slit width) in the Fe–O system. The spatial resolution achieved in our experiments was about 1.2 nm.

Acknowledgments

This work was supported by the Taiwan National Science Council through Grant nos. NSC 93-2120-M-009-009 and NSC 94-2120-M-009-010.

References

Colliex, C., Manoubi, T., Ortiz, C., 1991. Electron-energy-loss-spectroscopy near-edge fine structures in the iron–oxygen system. Phys. Rev. B 44, 11402–11411.

Egerton, R.F., 1996. Electron Energy-loss Spectroscopy in the Electron Microscope. Plenum Press, New York.

Egerton, R.F., 2003. New techniques in electron energy-loss spectroscopy and energy-filtered imaging. Micron 34, 127–139.

Egerton, R.F., Crozier, P.A., 1997. The effect of lens aberration on the spatial resolution of the energy-filtered TEM image. Micron 28, 117–124.

Jeanguillaume, C., Colliex, C., 1989. Spectrum-image: the next step in EELS digital acquisition and processing. Ultramicroscopy 78, 252–257.

Jeanguillaume, C., Trebbia, P., Colliex, C., 1978. About the use of electron energy-loss spectroscopy for chemical mapping of thin foils with high spatial resolution. Ultramicroscopy 3, 237–242.

Krivanek, O.L., Kundmann, M.K., Kimoto, K., 1995. Spatial resolution in EFTEM elemental maps. J. Microsc. 180, 277–278.

Leapman, R.D, Grunes, L.A., Fejes, P.L., 1982. Study the L_{23} edges in the 3d transition metals and their oxides by electron-energy-loss spectroscopy with comparisons to theory. Phys. Rev. B 26, 614–635.

Lo, S.-C., Kai, J.-J., Chen, F.-R., Chen, L.-C., Chang, L., Chang, C.-C., Ding, P.-J., Chin, B., Zhang, H., Chen, F.-S., 2001. Four-dimension dielectric property image obtain from electron spectroscopic imaging series. J. Electron Microsc. 50, 497–507.

Muller, D.A., Silcox, J, 1995. Delocalization in inelastic scattering. Ultramicroscopy 59, 195–213.

Reimer, L, 1995. Energy-filtering Transmission Electron Microscopy. Spring–Verlag, New York.

Snoeck, E., Serin, V., Fourmeaux, R., Zhang, Z., Freitas, P.P., 2004. Transmission electron microscopy evidence of the growth of a magnetite layer acting as a spin filter in CoFe/Al_2O_3/CoFe magnetic tunnel junctions. J. Appl. Phys. 96, 3307–3311.

Tsai, J.-S., Kai, J.-J., Chang, L., Chen, F.-R., 2004. Bandgap mapping for III–V quantum well by electron spectroscopy imaging. J. Electron Microsc. 53, 371–380.

Van Aken, P.A., Liebscher, 2002. Quantification of ferrous/ferric ratios in minerals: new evaluation schemes of Fe L_{23} electron energy-loss near-edge spectra. Phys. Chem. Miner. 29, 188–200.

Wang, Y.-X.J., Hussain, S.H., Krestin, G.P., 2001. Superparamagnetic iron oxide contrast agents: physicochemical characteristics and applications in MR imaging. Eur. Radiol. 11, 2319–2331.

Wang, Z.L., Yin, J.S., Zhang, J.Z., Mo, W.D., 1997. In situ analysis of valence conversion in transition metal oxides using electron energy-loss spectroscopy. J. Phys. Chem. B 101, 6793–6798.

Wang, Z.L., Bentley, J., Evans, N.D., 2000. Valence state mapping of cobalt and manganese using near-edge fine structures. Micron 31, 355–362.

Yang, J.-Y., Chen, F.-R., Kai, J.-J., 2002. Mapping of sp^2/sp^3 in DLC thin film by signal processed ESI series energy-loss image. J. Electron Microsc. 51, 391–400.